Semi-Automated Post-Processing Workflow for EGMS InSAR Data in Open-Pit and Dam Deformation Monitoring in the Presence of Sentinel-1 Winter Data Gaps

Pius Kipng’etich Kirui [1], Anna Reichstein[1], Andre Cahyadi Kalia [1]

[1] Federal Institute for Geosciences and Natural Resources (BGR), Stilleweg 2, 30655, Hannover, Germany – pius.kirui@bgr.de
[1]Federal Institute for Geosciences and Natural Resources (BGR), Stilleweg 2, 30655, Hannover, Germany – Anna.Reichstein@bgr.de
[1] Federal Institute for Geosciences and Natural Resources (BGR), Stilleweg 2, 30655, Hannover, Germany – andre.kalia@bgr.de

Keywords: InSAR post processing, Phase unwrapping error, Time series clustering, EGMS

Abstract

Deformation monitoring in open-pit mining operations is critical to ensure operational safety. Conventional in situ geodetic techniques yield predominantly sparse, point-based measurements, which restrict the ability to characterize deformation processes in a spatially comprehensive manner. In contrast, Interferometric Synthetic Aperture Radar (InSAR) can provide many measurements of ground displacements; however, its operational uptake is constrained by the complexity of data-processing workflows and the challenges associated with interpreting the resulting measurements. Although analysis-ready, InSAR-based ground-motion products have recently become available, their interpretation remains challenging for non-expert users. We propose a semi-automated workflow to post-process EGMS (European Ground Motion Service) displacement time series for operational monitoring of open pits and tailings dams in cold regions with seasonal data gaps, and we evaluate it using two test sites in Finland. In such environments, missing winter data can introduce phase-unwrapping artefacts in the time series, appearing as winter-only displacement offsets of approximately half the Sentinel-1 radar wavelength, which can easily be mistaken for real ground motion. The time series are pre-processed to identify and remove measurement points affected by phase-unwrapping errors. In order to support the interpretation of the data, subsequently time series clustering is performed. This is done either in a reduced-dimensional representation or directly in the full feature space. Cluster selection is automated using a combination of heuristic criteria and a custom metric based on temporal homogeneity and consistency. The findings show that the semi-automatically detected clusters are plausible with regards to a visual interpretation of the EGMS data.

1. Introduction

Deformation and stability monitoring of open pits and tailings dams is essential for ensuring mine safety and mitigating environmental and operational risks. Early detection of slope movements, potential slope failures, and dump instabilities helps prevent production interruptions, premature mine closure, and possible loss of life (Gong et al., 2021). Conventional in situ geodetic techniques such as GNSS and levelling offer high accuracy but are costly to maintain, unsuitable for continuous large-area monitoring, and restricted to predetermined observation points. As these fixed locations may not coincide with zones of potential slope instability, the resulting measurements may be not well positioned, and GNSS observations can additionally be affected by geometric constraints imposed by slope orientation (Chrzanowski & Szostak-Chrzanowski, 2009; Ma et al., 2012). InSAR, on the other hand, has become an attractive alternative thanks to free and open data policy e.g from the ESA SAR mission Sentinel-1, open-source processing software, and improved SAR acquisition and InSAR processing techniques that have significantly increased both the reliability and density of measurement points (Crosetto et al., 2020; Haupt et al., 2023). These developments have shifted InSAR from an on-demand tool to an operational deformation monitoring technique (Liao et al., 2020). InSAR processing, however, remains challenging for non-experts due to the extensive parametrization involved, while also being computationally intensive. In response, continental scale products are provided by the EGMS (Crosetto et al., 2020).

The large data volumes produced by the EGMS continue to present interpretation challenges, particularly for non-expert InSAR users (Barra et al., 2017). In cold regions, interpretation of InSAR results is further complicated by substantial winter data gaps, as SAR acquisitions during this period can become unusable due to snow coverage. These winter gaps introduce uncertainty in the InSAR-derived displacement time-series. Persistent Scatterer (PS) methods may show apparent deformation caused solely by unwrapping errors, resulting in an exaggeration of actual movement. Similarly, Small Baseline Subset (SBAS) approaches may become unreliable due to long temporal baselines or disconnected networks, producing biased or unstable solutions (Bui et al., 2020). In cold-region settings, systematic errors in EGMS ground-motion products must be corrected before the data can be reliably interpreted or used for post-processing. Phase-unwrapping artefacts are particularly challenging and can be characterized by biased displacement time series with magnitudes of about half the radar wavelength (Fan et al., 2025). Mitigating these artefacts enables the conversion of the data into application-ready information suitable for integration with other geohazard datasets (Navarro et al., 2020)

In their review, Crosetto et al. (2025) examine post-processing strategies used to enhance EGMS interpretability, ranging from conversion into GIS-ready formats (Festa & Del Soldato, 2023) to clustering-based analyses (Barra et al., 2017). In many studies clustering is applied to average velocities, often using the standard-deviation of the velocity as threshold (Mele et al., 2023). However, velocity-based clustering is unsuitable in areas with non-linear deformation. In such cases, time-series-based clustering provides a more suitable alternative. Nevertheless, its application is constrained by the high dimensionality of InSAR time-series data, which limits the applicability of clustering algorithms such as k-means or Hierarchical Density-Based

Spatial Clustering of Applications with Noise (HDBSCAN). Dimensional-reduction methods, including PCA, UMAP, and LSTM autoencoders e.g (Ansari et al., 2021; Rygus et al., 2023), are commonly used to reduce InSAR time-series dimensionality before clustering. However, identifying a reduced dimensionality that adequately represents the original temporal behaviour is challenging. For instance, maximising explained variance in PCA does not guarantee an optimal clustering dimensionality, as variance is not equivalent to separability, and current automated selection approaches, including UMAP-based heuristic separability metrics (Rygus et al., 2023) and variance-based criteria (Festa et al., 2023), may not reflect the underlying geophysical deformation processes.

Deformation is spatially autocorrelated and clustering solely in the temporal domain ignores spatial structure that directly influences clustering outcomes. This issue is particularly pronounced in cold regions, where InSAR time-series measurements are highly spatially heterogeneous. Temporal only approaches may therefore yield spatially incoherent groupings that cannot be attributed to meaningful causative mechanisms. Attempts to incorporate spatial information post-clustering, such as through variogram analysis (Tiwari & Shirzaei, 2024) serve as filtering steps rather than genuinely integrated spatio-temporal clustering and thus do not capture joint dependencies. Methods such as ST-DBSCAN have also been applied, but reported performance has been limited, likely due to challenges in parameter selection and in harmonising the temporal and spatial feature spaces (Prasanthi Malyala et al., 2025). Addressing both temporal and spatial complexity within a unified framework therefore is an open research question for producing meaningful clustering results. Building on this knowledge gap, the objective of this work is to develop a semi-automated post-processing framework for EGMS data in cold regions with large winter gaps, combining unwrapping-error mitigation with automated time-series-based clustering.

2. Data and Methods

Two test sites in Finland were selected to evaluate the proposed methodology as shown in Figure 1. In accordance with data-sharing agreements, the specific site names are withheld. Both locations include an active open-pit mine and an associated tailings storage facility (TSF) dam(s), as shown in Figure 1. EGMS Level 2A products serve as the input data, with a temporal coverage spanning 2019–2023 for both sites. Due to persistent seasonal snow cover in these northern regions, Sentinel-1 acquisitions during winter are excluded in the EGMS processing chain (EEA, 2025). Consequently, the available EGMS time series for Test Site A extends from April to late October, while Test Site B, located farther north, has a shorter snow-free period, with observations available from June to late October.

The workflow adopted in this study comprises three main stages: preprocessing of the L2A EGMS data, time-series domain clustering, and post-clustering refinement (Figure 2). Pre-processing is required to remove noisy measurement points. The time series also exhibit pronounced seasonal behaviour, with some points showing winter-only motion of up to half the Sentinel-1 wavelength (28 mm; Figure. 3), a pattern attributable to phase unwrapping errors caused by missing winter acquisitions. Measurement points affected by this behaviour were identified using the approach described in (“Spatio-temporal clustering for detection of active ground movement in open-pit and dam stability monitoring using EGMS data”, manuscript in preparation), which achieves detection rates of up to 92%.

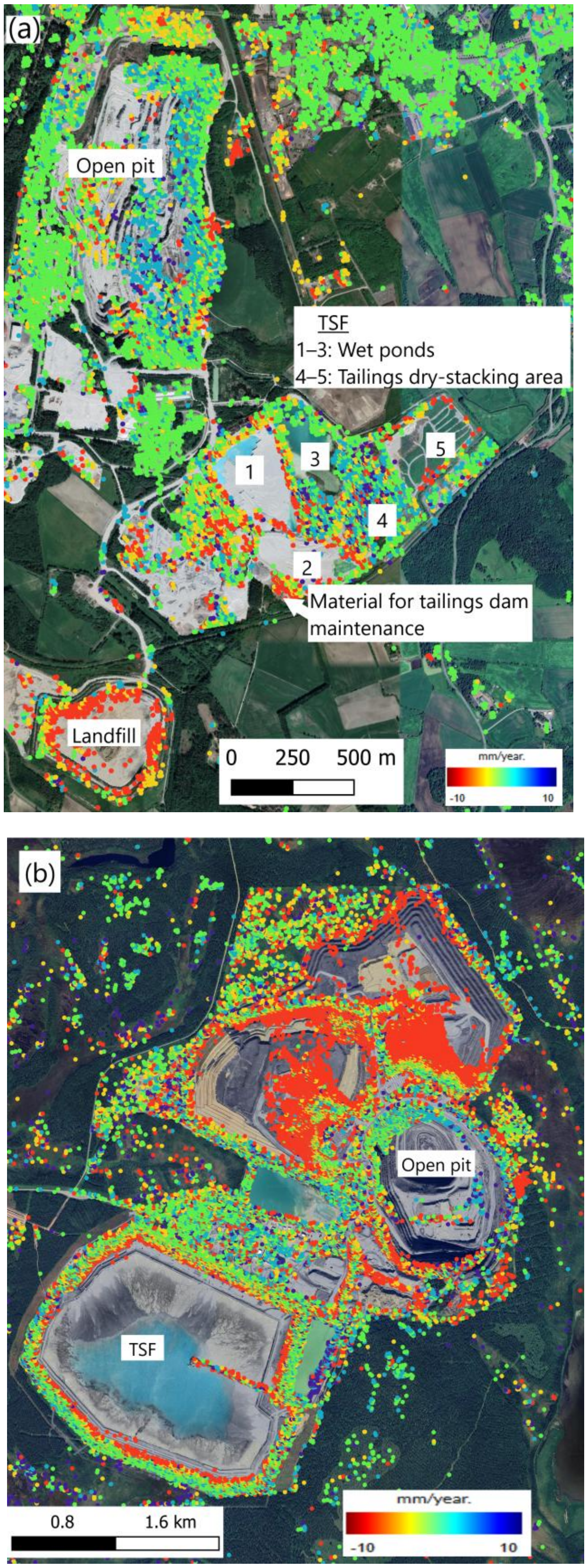

Figure 1. EGMS L2A data in study areas. Subfigure (a) shows study area A, and subfigure (b) shows study area B. Both sites include an open pit and a tailings dam.

The high spatial heterogeneity is addressed using a Temporal Coherence Index (TCI), defined as the product of temporal monotonicity and the lag-1 autocorrelation, capturing both directional persistence and short-term smoothness. The resulting TCI is then subjected to local Moran’s I with adaptive k-nearest neighbours, retaining only High–High measuring points. The selected time series are globally min-max normalised and serve as the input for clustering. Clustering is performed in the time-series domain, as the average displacement is not meaningful due to potential nonlinear movements. Two approaches are considered: Time Series K-Means (TSK-Means), which operates on the normalised raw time series, and methods such as k-means and HDBSCAN, which require prior dimensionality reduction.

Both the number of clusters and the dimensionality of the reduced feature space are determined automatically. Dimensionality reduction is guided by trustworthiness, while cluster selection for k-means and TSK-Means follows a two-stage procedure: first identifying ranges of k where solutions are stable, and then refining the selection based on cluster quality. This is because both k-means and and TSK-Means assign all points to clusters and do not identify noise. To ensure that the selected clustering solution reflects coherent and meaningful deformation behaviour, we propose a multi-metric cluster quality evaluation framework applied to all cluster candidates for each tested value of *k*. For every cluster, we compute four complementary metrics: an amplitude-stability metric (median IQR ratio), a temporal-shape similarity metric (mean pairwise Pearson correlation), a directional-agreement metric (increment-sign consistency with the centroid), and a fragmentation metric (cluster size). Thresholds for these metrics are not fixed; instead, they are derived from the pooled distribution of raw scores across all clusters and all *k* values using a median $\pm\,0.5\cdot$IQR rule, with the inequality direction matched to the expected behaviour of each metric. Each cluster is then assigned a quality tier based on the number of metrics it satisfies (4/4 = Quality, 3/4 = Partial, <3/4 = Poor). The final value of *k* is selected from the stability-filtered candidates as the solution that maximises the mean fraction of passed metrics while respecting minimum-cluster-size constraints.

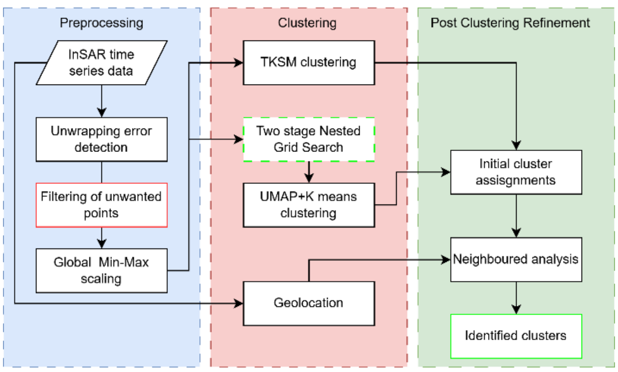

Figure 2. Schematic representation of the workflow.

Post-clustering refinement was applied to ensure spatially coherent and meaningful clusters. Because time-series clustering can produce mixed or spatially isolated assignments unrelated to actual deformation processes, a spatial neighbourhood analysis was used to remove these artefacts. A majority-vote filtering approach was used to identify and eliminate spatially heterogeneous or isolated cluster assignments. Points assigned to a given cluster were rejected when fewer than four neighbours of the same cluster were found within an 80 m radius, as such sparse occurrences are unlikely to represent a coherent deformation signal. The remaining, denser clusters were then subjected to a second majority-vote spatial filtering step, in which the dominant cluster label within the 80 m neighbourhood was retained. This procedure yields spatially coherent and interpretable deformation clusters.

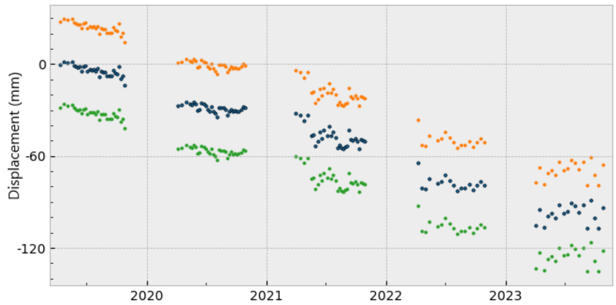

Figure 3. Displacement time series affected by a phase unwrapping error: the blue line shows the original LOS displacement time series, while the orange and green lines represent ±28 mm offsets (half the Sentinel-1 wavelength).

3. Results and Discussions

3.1 Cluster Selection in K-means and TSK-Means

For both k-means and TSK-Means, the number of clusters must be defined a priori, which poses a challenge in automated workflows. In the absence of a priori information, for example when the analysis is intended to distinguish only three broad classes such as stable ground, subsidence and uplift, identifying an appropriate cluster number becomes particularly difficult.

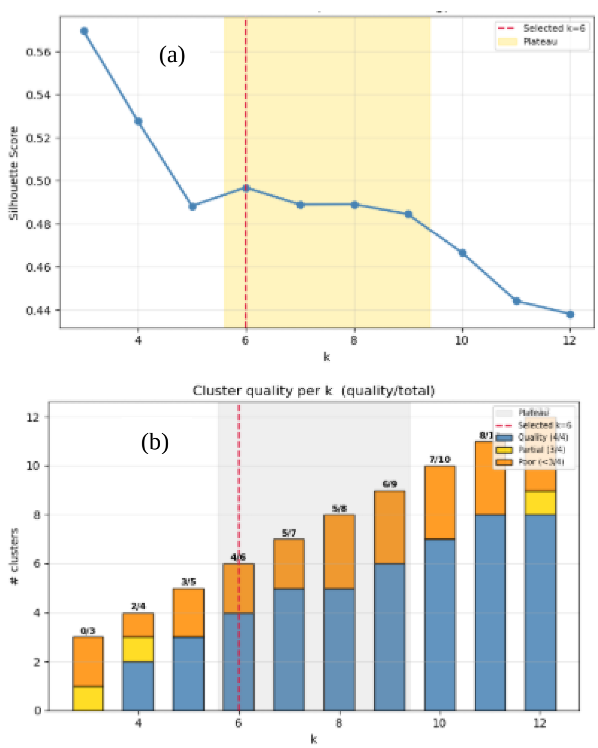

Figure 4. Cluster selection for k-means and TS-k-means. Subfigure (a) shows the selection of optimal k-means candidates, while subfigure (b) shows the selection of the final cluster combination based on cluster quality.

In order to find a reasonable number of clusters a heuristic metric such as the silhouette score is often used. However, as shown in Figure 4a, a high silhouette score does not necessarily translate into geological meaningful clusters. We find that solutions with very few clusters often achieve high silhouette scores, yet these clusters are highly heterogeneous and do not represent coherent time-series patterns. On the other hand, Figure 4a shows that there are regions where the silhouette score is relatively stable across a range of *k*. We use this stable region as the preliminary set of candidate cluster combinations. The final selection is then based on the cluster-quality criteria defined in Section 3. Although these combinations may be optimal in a numerical sense, they can still contain clusters that represent noise, since both k-means and TSK-Means are non-discriminative and assign all points to a cluster. The four-quality metrics therefore serve as a way to isolate noise-dominated clusters while retaining those that represent coherent deformation behaviour.

3.2 Application of K-means and TSK-Means Clustering to Site A

At Site A, applying k-means clustering to the UMAP-reduced feature space yielded four optimal clusters (Figure 5), whereas TSK-Means, operating directly on the full feature space, identified five (Figure 6). In both cases, the selection of the optimal cluster count was guided by silhouette scores and the four-quality metrics described in Section 3.

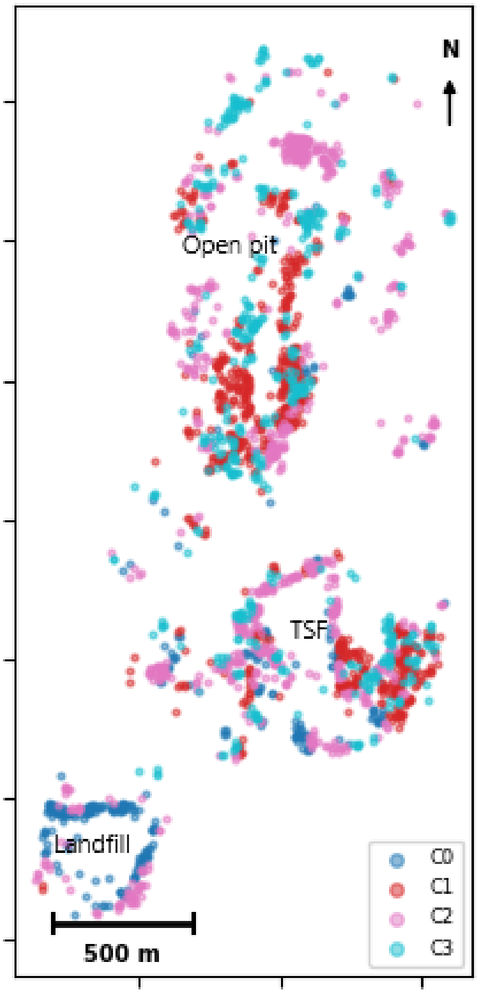

Figure 5. Spatial distribution of clusters derived from K-means clustering at Site A

The spatial distribution and temporal consistency of the clusters produced by both approaches align well with expected expert-interpreted ground movement behaviour. For example, as shown in Figure 5, k-means cluster 0 captures a distinct deformation signal along the landfill, while cluster 2 identifies a similar but less pronounced pattern along the TSF. Both clusters exhibit motion away from the satellite look direction, as shown by the cumulative LOS displacement time series (Figure 7). Conversely, cluster 1 represents motion toward the satellite along the west-facing slope of the open pit, again consistent with the corresponding time-series data. The remainder of the study area is largely represented by cluster 3, which characterizes stable behaviour with negligible cumulative displacement.

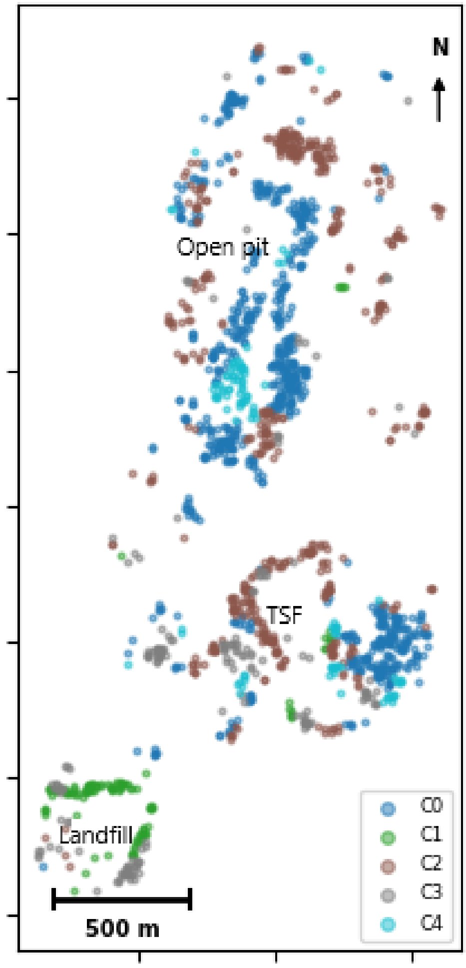

Figure 6. Spatial distribution of clusters derived from TSK-Means clustering at Site A.

Although the two approaches produce broadly comparable results, TSK-Means provides finer segmentation in specific regions. At the landfill, K-means generally assigns a single cluster, whereas TSK-Means resolves two distinct clusters. Similarly, on the west-facing slope at the open pit (Figure 6), TSK-Means identifies two clusters (0 and 4) exhibiting motion toward the satellite as shown in Figure 7, while K-means consolidates this behaviour into a single group. The substantial spatial overlap between the two methods is largely attributable to the predominantly linear displacement behaviour of measurement points at this site; under such conditions, both methods rely effectively on euclidean distance and therefore tend to produce similar partitions.

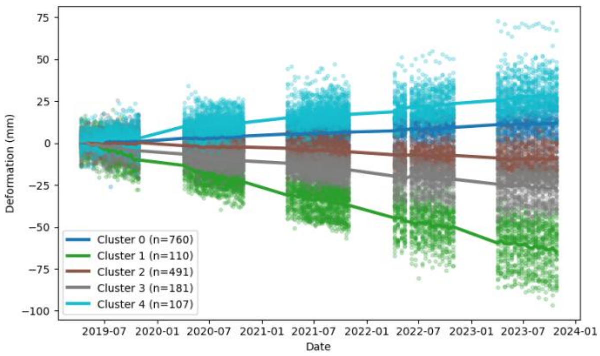

Figure 7. Time-series representatives from TSK-Means clustering, showing the median time series of each cluster alongside representative individual time series at site A.

The higher number of clusters produced by TSK-Means at site A is directly linked to its use of the full min-max-scaled time-series features, which preserves small differences in both deformation magnitude and temporal behaviour. These subtle variations are present in areas such as the landfill and the west-facing slope at the open pit (Figure 5 and Figure 6), where TSK-Means separates patterns that K-means groups together. In contrast, the UMAP reduction applied before K-means compresses the feature space, smoothing out fine-scale differences and often leading to fewer clusters. However**,** because most points at Site A exhibit simple, near-linear temporal trends, both methods still produce broadly similar spatial patterns, while TSK-Means retains enough detail to justify the additional segmentation observed in the results.

3.3 TSK-Means and HDBSCAN Clustering at site B

Time-series clustering at Site B reveals substantially more pronounced ground deformation than at Site A, both in terms of spatial extent and displacement magnitude as shown in figure 8. Whereas pronounced deformation at Site A is largely confined to the tailings dam, Site B exhibits widespread movement north of the open pit. This contrast is consistently captured by both TSK-Means and HDBSCAN (Figure 8 and 10), which produce broadly comparable cluster patterns with minor differences in spatial delineation of the clusters.

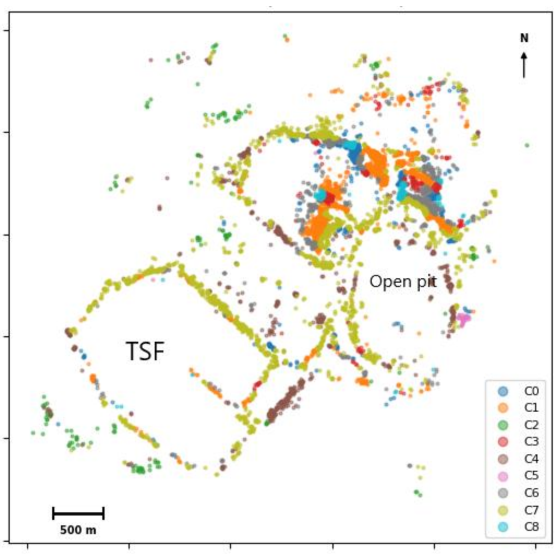

Figure 8 . Spatial distribution of clusters derived from TS-Kmeans clustering at Site B.

Both methods identify the open pit as the principal zone of deformation, characterized by multiple clusters exhibiting motion away in satellite LOS. Although these clusters share a generally linear temporal evolution, they differ in displacement rate and cumulative magnitude. TSK-Means resolves nine clusters, five moving away from the satellite LOS, one moving toward the LOS, and two that remain nearly stable—while HDBSCAN identifies eight five moving away from the satellite LOS, one moving toward the LOS, and two that remain nearly stable. The spatial distribution of these clusters is consistent across methods: the open pit hosts the majority of LOS-away motion whereas the dam and surrounding areas contain predominantly stable or low-motion clusters.

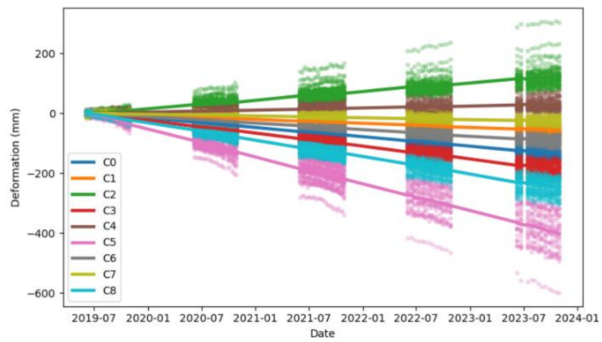

Figure 9. Time series representatives from TS k means clustering, showing the median time series of each cluster alongside representative individual time series at site B.

A key distinction between the two approaches arises from how HDBSCAN, operating in a reduced-dimensional feature space, compresses the displacement magnitude range within clusters. For example, TSK-Means isolates a cluster with cumulative displacement approaching –600 mm (Figure 9), whereas HDBSCAN assigns the same measurement points to a cluster with a mean cumulative displacement of approximately –200 mm (Figure 11). Thus, while both algorithms classify these points as deforming, TSK-Means preserves the magnitude contrast more explicitly, whereas HDBSCAN yields a more homogenized representation of displacement magnitude. Beyond working in reduced dimensional space, HDBSCAN is highly sensitive to parameter selection.

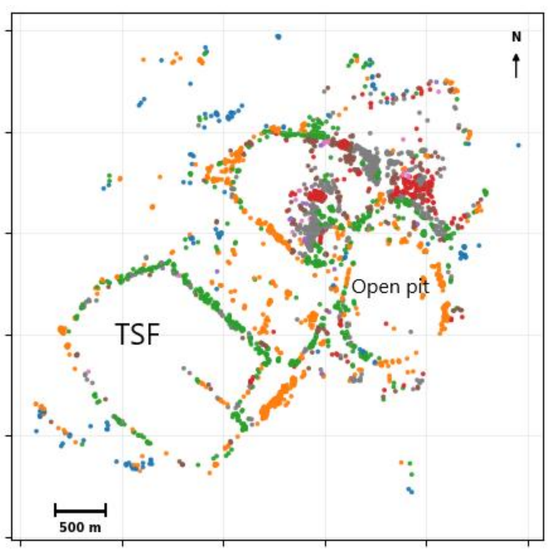

Figure 10. Spatial distribution of clusters derived from HDBSCAN clustering at Site B.

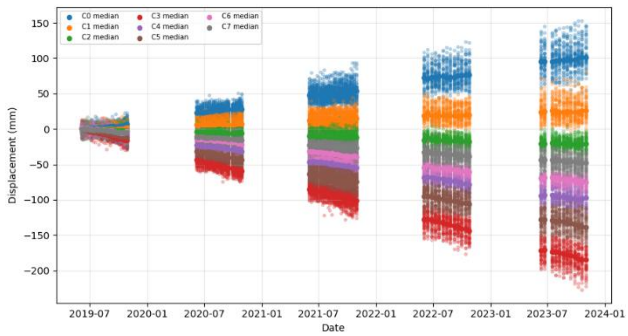

Figure 11. Time series representatives from HDBSCAN clustering, showing the median time series of each cluster alongside representative individual time series at site B.

For instance, even though we applied a grid-search optimization strategy, tuning HDBSCAN interdependent parameters is considerably more complex than the comparatively limited parameter space of TSK-Means. This complexity introduces additional uncertainty, as commonly used validity indices such as Density-Based Cluster Validation (DBCV) or the silhouette score do not reliably guarantee optimal partitions. And therefore, achieving geological meaningful results require imposing supplementary constraints like minimum number of clusters and expert-driven criteria during the optimization process.

3.4 Post Clustering

Given that clustering was performed exclusively in the time-series domain, an additional post-clustering refinement step was necessary to produce geologically meaningful cluster. This requirement arises because deformation in the test sites is assumed to be correlated not only temporally but also spatially. Therefore, the clusters must reflect similarity in temporal evolution as well as spatial autocorrelation. To this end, spatial filtering based on neighbourhood relationships was applied to the clusters for all the three approaches. For k-means and TSK-Means, in addition to spatial filtering, we employed the customized metrics used for cluster selection (as described in Section 3) to exclude clusters classified as “poor” and to remove measurement points that are located within clusters classified as “partial”. These customized metrics provide a systematic framework for the evaluation of individual clusters within an optimally selected cluster combination, thereby extending the capabilities of standard implementations of both k-means and TSK-Means.

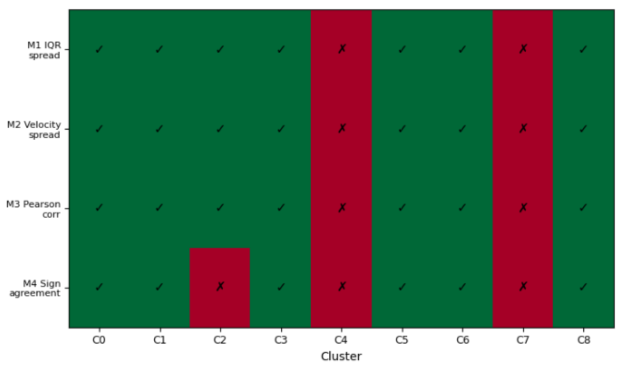

Figure 12 Classification of individual clusters within the optimally determined clustering solution, based on the four-evaluation metrics described in Section 3

For example, clusters 4 and 7 as shown in Figure 12 were classified as low-quality because they showed large interquartile ranges, low intra-cluster Pearson correlations, and strong spatial fragmentation, indicating they do not represent a physically interpretable or internally consistent deformation process. After discarding these clusters, the remaining clusters exhibited strong spatial homogeneity even prior to the application of explicit spatial filtering. Similarly, when a cluster is categorized as “partial”, this indicates that a subset of measurement points has likely been incorrectly assigned to that cluster. A potential reason could be because these points lie closest to the cluster centroid in feature space rather than sharing the same underlying deformation behaviour. For example, if a cluster is flagged as “partial” due to its IQR metric, points outside user-defined percentile limits (such as the 5^{th} and 95^{th} percentiles) can be removed, thereby excluding observations that fall outside the expected IQR range. This approach avoids discarding the entire cluster as noise and instead selectively removes inconsistent or noisy measurements, improving the quality of the resulting clusters.

4. Conclusions

We perform clustering in the time series domain without relying on velocity-based estimates, and our pre- filtering strategy avoids hard-coded thresholds in both the time series and velocity domains. Moran’s I–based neighbourhood analysis of the temporal index, defined as a function of monotonicity and temporal lag, effectively accounts for the majority of the EGMS-related noise present in our dataset. We show that k-means and TSK-Means yield broadly comparable cluster patterns that reflect a plausible deformation pattern at both the open pit and the tailings dam. This can be attributed to a predominantly linear displacement. Similarly, HDBSCAN reproduces the same overall pattern; however, the resulting clusters exhibit greater spatial homogeneity than those obtained with TSK-Means and k-Means in both sites. We attribute this to HDBSCAN’s ability to assign points that do not belong to any cluster structure or centroid as noise. In contrast, TSK-Means assigns all pixels to clusters, resulting in spatially heterogeneous groupings that require additional filtering of individual clusters to remove non-representative or noisy observations, even when using optimally selected cluster combinations. Our automated cluster selection framework identifies a reasonable? umber of clusters and provides a tailored metric that supports the post clustering. This is further enhanced by spatial filtering of the identified clusters, which compensates for the spatial heterogeneity that can arise because clustering is performed solely in the time series feature space. Future work could e.g. pursue more deterministic strategies, including spatial–temporal pre filtering, deterministic approaches for automated cluster selection or the integration of spatial attributes to enable fully joint spatio–temporal clustering.

References

Ansari, H., Ruβwurm, M., Ali, M., Montazeri, S., Parizzi, A., & Zhu, X. X. (2021). InSAR displacement time series mining: A machine learning approach. *2021 IEEE International Geoscience and Remote Sensing Symposium IGARSS*, 3301–3304.

Barra, A., Solari, L., Béjar-Pizarro, M., Monserrat, O., Bianchini, S., Herrera, G., Crosetto, M., Sarro, R., González-Alonso, E., & Mateos, R. M. (2017). A methodology to detect and update active deformation areas based on Sentinel-1 SAR images. *Remote Sensing*, *9*(10), 1002.

Bui, L. K., Featherstone, W. E., & Filmer, M. S. (2020). Disruptive influences of residual noise, network configuration and data gaps on InSAR-derived land motion rates using the SBAS technique. *Remote Sensing of Environment*, *247*, 111941. https://doi.org/https://doi.org/10.1016/j.rse.2020.111941

Chrzanowski, A., & Szostak-Chrzanowski, A. (2009). Deformation monitoring surveys-old problems and new solutions. *Reports on Geodesy*, 85–103.

Crosetto, M., Crippa, B., Mróz, M., Cuevas-González, M., & Shahbazi, S. (2025). Applications based on EGMS products: A review. *Remote Sensing Applications: Society and Environment*, *37*, 101452. https://doi.org/https://doi.org/10.1016/j.rsase.2025.101452

Crosetto, M., Solari, L., Mróz, M., Balasis-Levinsen, J., Casagli, N., Frei, M., Oyen, A., Moldestad, D. A., Bateson, L., & Guerrieri, L. (2020). The evolution of wide-area DInSAR: From regional and national services to the European Ground Motion Service. *Remote Sensing*, *12*(12), 2043.

European Environment Agency (EEA). (2025, August 7). European Ground Motion Service (EGMS) - Algorithm Theoretical Basis Document (Version 4). Copernicus Land Monitoring Service. https://library.land.copernicus.eu/products/European_Ground_Motion_Service_Algorithm_Theoretical_Basis_Document_v4.pdf

Fan, C., Liu, L., Zhao, Z., & Mu, C. (2025). Pronounced underestimation of surface deformation due to unwrapping errors over Tibetan Plateau permafrost by Sentinel-1 InSAR: Identification and correction. *Journal of Geophysical Research: Earth Surface*, *130*(3), e2024JF007854.

Festa, D., & Del Soldato, M. (2023). EGMStream, a desktop app for EGMS data downstream. *Remote Sensing*, *15*(10), 2581.

Festa, D., Novellino, A., Hussain, E., Bateson, L., Casagli, N., Confuorto, P., Del Soldato, M., & Raspini, F. (2023). Unsupervised detection of InSAR time series patterns based on PCA and K-means clustering. *International Journal of Applied Earth Observation and Geoinformation*, *118*, 103276.

Gong, C., Lei, S., Bian, Z., Tian, Y., Zhang, Z., Guo, H., Zhang, H., & Cheng, W. (2021). Using time series InSAR to assess the deformation activity of open-pit mine dump site in severe cold area. *Journal of Soils and Sediments*, *21*(11), 3717–3732.

Haupt, S., Engelbrecht, J., Sibolla, B., & Mdakane, L. W. (2023). Time series insar analysis for slope stability monitoring using sentinel-1 in open pit mining. *The International Archives of the Photogrammetry, Remote Sensing and Spatial Information Sciences*, *48*, 945–951.

Liao, M., Balz, T., Rocca, F., & Li, D. (2020). Paradigm changes in Surface-Motion estimation from SAR: Lessons from 16 years of Sino-European cooperation in the dragon program. *IEEE Geoscience and Remote Sensing Magazine*, *8*(1), 8–21.

Ma, F., Zhao, H., Zhang, Y., Guo, J., Wei, A., Wu, Z., & Zhang, Y. (2012). GPS monitoring and analysis of ground movement and deformation induced by transition from open-pit to underground mining. *Journal of Rock Mechanics and Geotechnical Engineering*, *4*(1), 82–87. https://doi.org/https://doi.org/10.3724/SP.J.1235.2012.00082

Mele, A., Crosetto, M., Miano, A., & Prota, A. (2023). Adafinder tool applied to EGMS data for the structural health monitoring of urban settlements. *Remote Sensing*, *15*(2), 324.

Navarro, J. A., Tomás, R., Barra, A., Pagán, J. I., Reyes-Carmona, C., Solari, L., Vinielles, J. L., Falco, S., & Crosetto, M. (2020). ADAtools: Automatic detection and classification of active deformation areas from PSI displacement maps. *ISPRS International Journal of Geo-Information*, *9*(10), 584.

Prasanthi Malyala, L., Krishnan, S. B., Prasad, Kv., & Chakrabarti, P. (2025). A deep embedded clustering approach for detecting trend class using time-series sensor data. *Knowledge-Based Systems*, *320*, 113609. https://doi.org/https://doi.org/10.1016/j.knosys.2025.113609

Rygus, M., Novellino, A., Hussain, E., Syafiudin, F., Andreas, H., & Meisina, C. (2023). A clustering approach for the analysis of InSAR Time Series: Application to the Bandung Basin (Indonesia). *Remote Sensing, 15*(15), 3776.

Tiwari, A., & Shirzaei, M. (2024). A novel machine learning and deep learning semi-supervised approach for automatic detection of InSAR-based deformation hotspots. *International Journal of Applied Earth Observation and Geoinformation, 126*, 103611. https://doi.org/https://doi.org/10.1016/j.jag.2023.103611

Acknowledgements

This work is carried out within the MultiMiner and GoldenRAM projects. The Multi-source and Multi-scale Earth Observation and Novel Machine Learning Methods for Mineral Exploration and Mine Site Monitoring (MultiMiner) project is funded by the European Union's Horizon Europe research and innovation actions programme under Grant Agreement No. 101091374, and GoldenRAM is funded by the European Union's Horizon Europe innovation actions programme under Grant Agreement No. 101138153.